Remote Sensing Applications: Society and Environment 26 (2022) 100728

Contents lists available at ScienceDirect

Remote Sensing Applications: Society and Environment

journal homepage: www.elsevier.com/locate/rsase

Pansharpened landsat 8 thermal-infrared data for improved Land Surface Temperature characterization in a heterogeneous urban landscape

Terence Darlington Mushore [a,b,*], Onisimo Mutanga [a], John Odindi [a], Vanessa Sadza [b], Timothy Dube [c]

[a] Discipline of Geography, School of Agricultural, Earth and Environmental Sciences, University of KwaZulu-Natal, P/Bag X01, Scottsville, Pietermaritzburg, 3209, South Africa
[b] Department of Space Science and Applied Physics, Faculty of Science, University of Zimbabwe, MP167, Mt Pleasant, Harare, Zimbabwe
[c] Department of Earth Sciences, Institute for "Water" Studies, University of the Western Cape, Private Bag X17, Bellville, 7535, South Africa

ARTICLE INFO

Keywords:
Pansharpening
LST
Landsat 8
Remote sensing
Urban micro climate
LULC

ABSTRACT

Reliable urban Land Use Land Cover (LULC) and Land Surface Temperature (LST) characterization are important for land use planning as well as climate and thermal impact analysis in cities. High resolution LULC and LST datasets are required for detailed spatial analysis such as understanding the contribution of small LULC fragments to thermal characteristics of the entire urban landscape. To date, detailed analysis of urban surfaces using satellite imagery has been hindered by low to moderate spatial resolution of freely available sensors of past and existing missions. Hence, this study sought to investigate the potential of pansharpening Landsat 8 data in improving LULC mapping and LST characterization in Bulawayo metropolitan city, Zimbabwe. Six LULC classes namely; bare area, built-up, low density, dense forest, grasslands and water bodies were considered for the study and respective spatially-explicit locational information (GPS coordinates) class samples identified. Supervised image classification using the Support Vector Machines algorithm was adopted for the un-pansharpened (30m) and separately using different pansharpened (i.e. Brovey, Simple Mean, ESR, IHS and Gram-Schmidt) datasets (15m) as input. Results indicated improved discriminability of LULC and LST features as well as increased classification accuracy from all pansharpening methods when compared to the 30m resolution data. Average inter-class separability increased from 1.577 using original data to 1.863 after pansharpening. The simple mean method showed the highest classification accuracy (92.13%), outperforming un-pansharpened data (89.77%) and other pansharpening methods (89.45–91.75%). Pansharpened data showed better accuracy in LST spatial characterization than un-pansharpened thermal data. For each LULC class, mean LST was slightly higher before, than after pansharpening, by between 0.1 and 1 °C. The study further established that pansharpening based on simple mean method did not compromise the spatial correlation between LULC and LST. These findings present a great improvement towards accurately mapping LULC and LST in heterogeneous urban landscapes.

* Corresponding author. Discipline of Geography, School of Agricultural, Earth and Environmental Sciences, University of KwaZulu-Natal, P/Bag X01, Scottsville, Pietermaritzburg, 3209, South Africa.
E-mail address: MushoreT@ukzn.ac.za (T.D. Mushore).

https://doi.org/10.1016/j.rsase.2022.100728
Received 18 June 2021; Received in revised form 17 December 2021; Accepted 5 March 2022
Available online 8 March 2022

1. Introduction

Reliable urban Land Use Land Cover (LULC) and Land Surface Temperature (LST) characterization are important for land use planning, as well as climate and thermal impact analysis in cities (Herold et al., 2002; Wang et al., 2012; Wilson et al., 2003; Zhou et al., 2011). Detailed delineation enables identification of LULC fragments of different sizes, valuable in quantifying the contribution of LULCs to associated physical or social phenomena (Saaroni et al., 2000; Voogt, 2000; Waqar et al., 2012; Weng and Yang, 2004). Typically, energy balance at any location depends on LULC, which varies over short distances on urban landscapes (Weng et al., 2007). However, technological limitations have impeded the acquisition of freely available high resolution multispectral and thermal imagery necessary for urban thermal characterization (Huang et al., 2015). Although a number of moderate resolution datasets (e.g. archival records of the Landsat series and MODerate resolution Imaging Spectrometer [MODIS]) are readily and freely available (Yuan et al., 2005; Owen et al., 1998), they are characterized by low spatial resolution, inadequate for monitoring heterogonous landscapes. This renders moderate resolution data unsuitable for resolving the often complex urban surface types. Whereas the adoption of high spatial and spectral resolution data has proved effective for Land Surface Temperature (LST) analysis (Mallick et al., 2013), scarcity of such data has impeded their use for deriving thermal characteristics on urban physical and natural processes. Although Liu and Weng (2009) found 30m resolution optimum to study the relationship between LULC and LST, finer resolution is required to adequately capture surface complexities in urban areas. For example, the width of roads in cities is commonly around 10–30m, such that at the resolution of Landsat 8 thermal imagery (even after resampling to 30m), most pixels are mixed and not necessarily pure (Goldreich, 2006). In addition, while the commonly available moderate resolution datasets such as the Landsat series, the MODIS and the Advanced Spaceborne Thermal Emission and Reflection Radiometer (ASTER) have an advantage of simultaneous optical and thermal data acquired at temporal resolution adequate to determine monthly, seasonal and long term land surface changes (Yuan et al., 2005; Owen et al., 1998), the optical (finer) and thermal (coarser) spatial resolution data mismatch imply a need for enhancement. Thermal data from spaceborne sensors is commonly obtained at a coarser resolution than optical data. The Landsat 8 mission for instance has eight reflective bands at 30m resolution, a panchromatic band at 15 m resolution and two thermal infrared bands at a coarser 100m resolution before resampling (Dube, 2016; Johnson, 2014). Although thermal data is downloaded at a resolution of 30m, it still suffers from the insufficiency caused by resampling (interpolating) from large to small pixels. For instance, 9 pixels of the new 30m resolution grid extract values from the same pixel of the 100m grid using cubic-convolution-based resampling method. Cubic convolution calculates an output cell value for a four by four block surrounding the input cell (Arif and Akbar, 2005). The procedure solves the problem of difference in pixel orientation between the original thermal and the 30m multispectral data but not the loss of spatial details. Mismatch still exists between the LULCs on the ground and their actual influence on LST. Typically, urban LULC is composed of heterogeneous patches of different shapes and sizes (Liu and Weng, 2009), with thermal properties of small size patches engulfed by contribution from larger patches. Hence, studies like Zhang et al. (2009) used vegetation patches exceeding 60 m by 60m to relate to LST derived from Landsat ETM thermal infrared data in Nanjing City, China. Weng et al. (2004) and Xiao et al. (2007) also observed that the correlation between LST and Normalized Difference Vegetation Index (NDVI) and percentage Impervious Surface Area (ISA) increased when the indices were generalized to the resolution of Landsat ETM + thermal data. Their findings are also consistent with Kato et al. (2010) who note that at 90m resolution of ASTER thermal data, it was difficult to determine the influence of buildings, street trees, rivers, parks and shadows of buildings on LST. Since finer resolution data enables more detailed feature analysis, (Liu and Weng, 2009), Agam et al., 2007 used a relationship between NDVI and LST to improve thermal data spatial resolution in Central Iowa, while Bai et al. (2015) used a spatio-temporal fusion technique of combining Landsat ETM+ with MODIS data to derive daily LST at 30m resolution in Guangzhou, China. Whereas the above named examples demonstrate great effort to solve the mismatch between thermal and optical data from freely available moderate resolution datasets, further investigation to improve LULC and LST spatial analysis in urban landscapes is necessary.

Data fusion (pansharpening) is known to be the most cost-effective way of improving spatial resolution of remotely sensed imagery (Gilbertson et al., 2017; He et al., 2014; Johnson, 2014). Pansharpening involves merging of multispectral data with higher spatial resolution panchromatic data, resulting in a new set of multispectral data with improved spatial resolution. This technique has been successfully adopted to improve moderate resolution datasets and further enhance high resolution datasets for sub-pixel and object-oriented analysis (Gilbertson et al., 2017; Johnson, 2014; Marangoz et al., 2006). The technique provides significant advantages over use of original coarse resolution data such as improved system reliability, classification accuracy and enhanced visualization (He et al., 2014; Johnson, 2014). Studies have demonstrated that pansharpening does not compromise data quality (Ayhan and Atay, 2012; Marangoz et al., 2006; Sarp, 2014; Xu et al., 2017). A study by Xu et al. (2017) for instance demonstrated that the correlation between un-pansharpened and pansharpened spectral bands increases, with a decreased Root Mean Square Error (RMSE). Hence, literature suggests that pansharpening improves retrievals, which in turn improves the mapping accuracy (Jawak and Luis, 2013; Marangoz et al., 2006; Xu et al., 2017). Gilbertson et al., (2017) for instance observed that pansharpening increased accuracy of LULC classification by 15% in Cape Winelands, South Africa while Xu et al. (2017) recorded a decrease in RMSE in estimation of impervious surfaces of between 0.1 and 0.3% in Yuen Long, Sha Tin and Central region in Hong Kong. Jawak and Luis (2013) identified small water bodies and individual trees by pansharpening multispectral WorldView data from 1.86 to 0.46m in Rio de Janeiro, on a strip of Brazil's Atlantic coast. Despite the benefits of pansharpening for land surface analysis, its potential for improving spatial characterization of urban LST remains largely unexplored. On the other hand, the recently launched Landsat 8 is characterized by improved radiometric resolution (U.S. Geological Survey, 2019) which, combined with pansharpening, presents a unique opportunity for retrieval of enhanced spatial and radiometric details. Due to its free availability, the resultant spatial resolution improvements offer a valuable opportunity for detailed urban thermal analysis in cases of limited or no financial resources.

In previous studies, the use of different algorithms have shown mixed results, which necessitates determination of the best

algorithms for a given dataset, purpose and location (Jawak and Luis, 2013; Sarp, 2014; Xu et al., 2017). Using IKONOS (5.8m for multispectral and 1m for panchromatic) and Quickbird (2.4m for multispectral and 0.6m for panchromatic) data in the northeastern part of Sisli municipality, Istanbul, Turkey, Principal Component yielded the best results followed by Gram Schmidt, Brovey and Intensity Hue Separation, respectively (Sarp, 2014). In another study, Jawak & Luis (2013), using WorldView-2 (0.46m for panchromatic and 1.86m for multispectral bands) data, noted that Gram Schmidt yielded the best classification accuracy followed by Principal Component and Intensity Hue Separation, respectively. Using WorldView-2 in Hong Kong, Gram Schmidt gave best accuracies in Yuen Lang and Sha Tin regions while best accuracy in the central areas was from Principal Component Analysis (Xu et al., 2017). A further comparison of pansharpening methods for improving urban surface characterization and thermal analysis will therefore be of great interest.

Image classification is the most common and basic remote sensing application. Quantitatively, there are several derived indices used to determine the characteristics of land surface materials in space and time. The NDVI proposed by Tucker (1979) is the most widely used indices due to ease of computation and capabilities to detect vegetation abundance, health and vigor (Bhandari et al., 2012; Buyantuyev et al., 2007; Shakya and Yamaguchi, 2010). In thermal analysis, a number of studies have used NDVI to quantify the effects of vegetation abundance and spatial structure on LST and Urban Heat Island (UHI) intensities and patterns (Chen et al., 2006; Gusso et al., 2014; Mallick, 2014; Mallick et al., 2013; Omran, 2012; Owen et al., 1998; Shi et al., 2015; Wu et al., 2014; Yuan and Bauer, 2007). In most of these studies, an inverse relationship between NDVI and LST that vary in place and season have been observed. In Mallick et al. (2013), for instance, an R-squared of 0.5154 was obtained while, Omran (2012) recorded a low correlation coefficient of −0.15 between NDVI and LST. On the other hand, Urban Index (UI) is known to be effective in delineating built-up areas and providing a quantitative measure of urbanization extent, which is directly correlated with LST (As-syakur et al., 2012; Kawamura et al., 1998; Mushore et al., 2017a,b; Sekertekin et al., 2018; Stathakis et al., 2012). In Harare Metropolitan city, for instance, Mushore et al. (2017) observed that UI gave the highest correlation with LST compared to 14 other indices, including NDVI. Using Landsat 8 data, NDVI and UI are retrieved at 30mfrom reflective data requiring further refinement to match complex heterogeneity in urban areas. High resolution data has potential to influence vegetation indices by adequately separating urban materials based on vegetation abundance and urbanization extents. As such, the effect of pansharpening thermal and optical data on the relationship between LST and NDVI as well as between LST and UI needs investigation.

In addition to testing the potential to improve spatial details for thermal analysis, identification of the best algorithm suited for a study area (Bulawayo Metropolitan City in Zimbabwe) is of great value. Hence, the objectives of this study were (i) to compare and test the potential of five pansharpening methods (Brovely, ESRI, Gram Shmidt, Simple Mean and Intensity Hue Saturation) to improve LULC and LST retrieval using LANDSAT 8 data, (ii) to establish the effect of pansharpening on the link between LULC and LST quantitatively as well as qualitatively and (iii) to determine the LULC and LST spatial patterns of the Bulawayo Metropolitan city in Zimbabwe. The study provides a highlight and implementation of the five pansharpening methods comparing their effect on LULC mapping accuracy and LST spatial structure retrieval at 15m using Landsat 8 data in Bulawayo. Based on mapping accuracy and visual assessment, the study compares the quality of un-pansharpened with pansharpened retrievals. Variations of LST with LULC are also investigated before and after pansharpening, qualitatively using LULC classification and quantitatively using the urban index.

2. Materials and methods

2.1. Study area

This study was conducted in Bulawayo (Fig. 1), the second largest city in Zimbabwe with approximately 1 million inhabitants. Fig. 1 demonstrates the heterogeneous nature of the city especially in the western areas where buildings and vegetation either coexist or are within short distances. The city is located at latitude −20.15° and longitude 28.51° and an elevation of 1358m above sea level. The area is characterized by a hot wet summer from October to March, with average temperatures of 25 °C and a cool dry season with

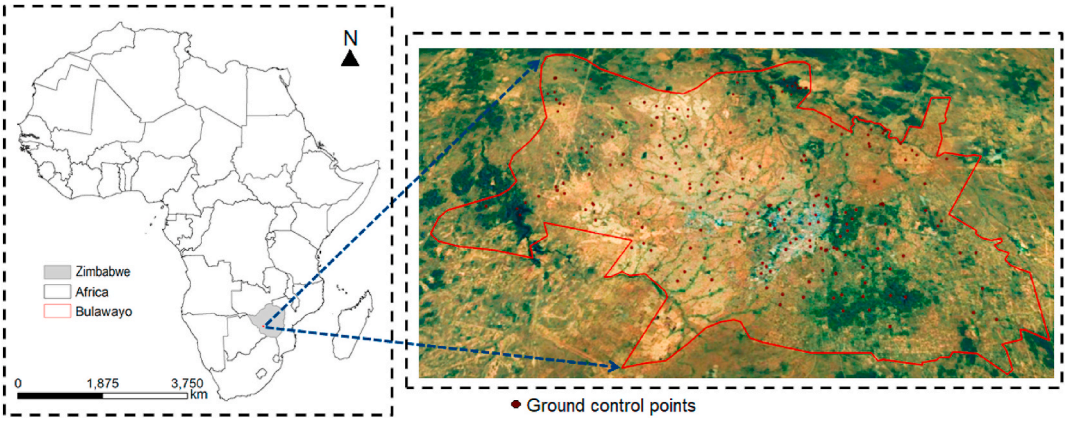

Fig. 1. Location of Bulawayo in Zimbabwe and image for Bulawayo extracted from Google Earth as well as the distribution of ground control points used for LULC mapping.

an average temperature of 15 °C for the rest of the year (Mutengu et al., 2007). The area lies in the semi-arid region of Zimbabwe that often receives erratic below average annual rainfall. The average annual rainfall is about 600 mm that ranges from 199.3 to 1258.8 mm, with a standard deviation of 202.3 mm. Most of the rain falls from December to February. Being close to the Kalahari Desert, Bulawayo is vulnerable to droughts and rainfall varies sharply from one year to another (Gumbo et al., 2003; Muchingami et al., 2012).

2.2. Field data collection

Six distinct LULC classes were identified in Bulawayo metropolitan city during a field survey and also with the aid of high resolution GoogleEarth imagery. Coordinates of sample points to represent each LULC type were collected using a handheld GPS in a stratified random sampling approach. The field survey was carried out between 18 and 27 October in 2020 and a minimum of fifty points were obtained for each class. A detailed description of LULC classes considered is summarized in Table 1. The points for each class were split into 70% for training (supervised classification) and 30% for accuracy assessment using stratified random sampling method (Adelabu et al., 2013). In this study, remote sensing data from Landsat 8 were subjected to different pansharpening methods while the same field collected data was used as ground truth. This was done to avoid introducing other variables by changing field data between analysis which could influence mapping accuracy other than the effect of pansharpening methods that were under investigation. The field data were collected at a time close to that of the acquisition of Landsat 8 data to minimize errors due to differences in time between imagery and ground truth data.

2.3. Remotely sensed datasets

Cloud-free Landsat 8 imagery (path/row 171/74) for the hot season acquired on 16 September, 19 October and 5 November in 2020, were freely downloaded from the United States Geological Survey's (USGS) Earth explorer website (www.earthexplorer.usgs.gov). Landsat 8 provides 8 reflective bands at a resolution of 30m, a panchromatic band (also in the reflective range) at 15m resolution and two thermal bands at 100m (downloaded at a resolution of 30m after resampling using a cubic convolution) - (Acharya and Yang, 2015; Roy et al., 2014). The hot and dry period (mid-September to mid-November) was chosen as it is conducive for land surface analysis due to the high likelihood of obtaining cloud free satellite imagery. Specifically, this period corresponded with field data collection. Atmospheric correction of the reflective bands was done using the Fast Line-of-sight Atmospheric Analysis of Spectral Hypercubes (FLAASH) tool in the ENVI (licensed) version 4.7 software. In the FLAASH module, the atmospheric model was set to tropical (because Zimbabwe experiences a tropical climate) while the urban aerosol model (because the study covered an urban area) was used. Multispectral image classification requires that the input bands be combined into a single file made from the overlays. This was achieved using the layer stacking tool in ENVI software set to the inclusive range. Thermal infrared data (Band 10 and 11 of Landsat 8) and the panchromatic band were not included in layer stacking as they were set aside for the computation of LST and pansharpening processes, respectively. Band 10 was used for LST retrieval while Band 11 was not employed throughout the study because it shows instability in values (Acharya and Yang, 2015). Since the purpose of the study was to investigate the effect of pansharpening on urban surface characterization, the multi-layer stack of reflective data was subjected to five different pansharpening methods namely Brovely, ESRI, Gram Schmidt, Simple Mean and Intensity Hue Saturation. This was done to assess the influence of the pansharpening method on resultant data characteristics and urban mapping accuracy. Focus was only placed on pansharpening methods that are contained in a Geographical Information Systems (GIS) environment for ease of processing. Brief descriptions of the adopted pansharpening methods are provided below. During pansharpening in ArcGIS software, weights of 0.334, 0.330 and 0.334 were assigned to the Red, Green and Blue bands for all the methods, respectively.

2.3.1. Brovey pansharpening

The Brovey pansharpening method uses one panchromatic band and three Multispectral (MS) bands to produce three pansharpened Multispectral bands. The approach is easy to compute and offers fast processing times. It fuses multispectral data with panchromatic band following the equations:

$$\boldsymbol{Red} = \frac{\boldsymbol{Red}}{\boldsymbol{Blue}(\boldsymbol{in}) + \boldsymbol{Green}(\boldsymbol{in}) + \boldsymbol{Red}(\boldsymbol{in})} \times \boldsymbol{Pan} \quad (1)$$

$$\boldsymbol{Green} = \frac{\boldsymbol{Green}}{\boldsymbol{Blue}(\boldsymbol{in}) + \boldsymbol{Green}(\boldsymbol{in}) + \boldsymbol{Red}(\boldsymbol{in})} \times \boldsymbol{Pan} \quad (2)$$

Table 1
LULC classes.

Class	Description
Bare area	Area with no buildings, grass, trees or any structures
Densely built-up	Densely built-up areas including Central Business District and Industrial area where imperviousness is marked
Dense forest	Dense forest cover dominated by dense trees
Low to medium built-up	Low to medium density residential areas (including sparse forests) with more greenery than densely built-up areas
Grassland	Area dominated by grass and small shrubs
Water body	Water bodies like lakes, ponds dams and rivers

$$Blue = \frac{Blue}{Blue(in) + Green(in) + Red(in)} \times Pan \quad (3)$$

where Red, Green, and Blue are the MS bands which are pansharpened in RGB; Red (in), Green (in), and Blue (in) are the low resolution MS bands in RGB (Zhang and Mishra, 2014).

2.3.2. Environmental Systems Research Institute (ESRI) method

The ESRI method first produces a weighted image using the MS bands. An adjustment image (ADJ) is then produced by subtracting the grey values of the weighted image from those of the original panchromatic image. Finally, ADJ is added to each of the individual MS bands, respectively, to generate individual pansharpened MS bands. ESRI Pansharpening method uses the following equations to generate a pansharpened image:

$$ADJ = Pan - W \quad (4)$$

$$Red_{out} = Red_{in} + ADJ \quad (5)$$

$$Green_{out} = Green_{in} + ADJ \quad (6)$$

$$Blue_{out} = Blue_{in} + ADJ \quad (7)$$

$$NIR_{out} = NIR_{in} + ADJ \quad (8)$$

where *ADJ* is the image that has been attuned; *W* is a weighted mean image of the MS bands; Pan is the panchromatic image with high spatial resolution; Red_{out}, $Green_{out}$, $Blue_{out}$ and NIR_{out} are the R, G, B, and NIR MS bands that are pansharpened; Red_{in}, $Green_{in}$, $Blue_{in}$, and NIR_{in} are the *R, G, B*, and *NIR* MS bands with low resolution (Xu et al., 2013; Zhang and Mishra, 2014).

2.3.3. Gram-Schmidt method

The Gram-Schmidt method produces a replicated pansharpened low resolution image through weighted addition of red, blue, green, and near-infrared MS bands. The weights for the four MS bands are computed on the basis of the sensor's optical transmission and spectral reaction for the Panchromatic (Pan) band and four MS bands. A Gram Schmidt conversion is then used to the replicated low resolution Pan and the low resolution MS bands, starting with the replicated panchromatic as the first band. The pan image with high resolution is changed to fit the first band of Gram Schmidt transformed bands. Then, the replicated Pan is used to substitute the first band of the Gram Schmidt altered bands and an inverse Gram Schmidt transformation used to produce pansharpened MS bands. The equation for calculating the replicated low resolution Pan image is:

$$Pan_{syn} = (B \times B_W) + (G \times G_W) + (R \times R_W) + (NIR \times NIR_W) \quad (9)$$

where Pan_{syn} is the replicated *Pan* image with low resolution *R, G, B*, and *NIR* being the MS bands; and B_w, G_w, R_w; and NIR_w are the weights for the *R, G, B*, and *NIR* bands, respectively (Zhang and Mishra, 2014; Belfiore et al., 2016). The colors of the composite RGB pansharpened bands are almost identical to the corresponding original images. Gram-Schmidt method is more robust to spatial misalignment of the bands than most other pansharpening methods because all transform coefficients are computed in the low MS resolution (Parente and Santamaria, 2014).

2.3.4. Intensity-Hue-Saturation (IHS)

The Intensity-Hue-Saturation (IHS) method is based on RGB (Red-Green-Blue) to IHS space transformation. The intensity component *I* is substituted by the panchromatic image because of their similarity and the inverse transformation (from IHS to RGB space) is applied (Belfiore et al., 2016). IHS sharpening converts *R, G* and *B* bands of MS image into IHS components, whose histogram is matched with intensity component of original multispectral image (Choi et al., 2006; Sarp, 2014; Tu et al., 2004). Inverse transformation is then performed to obtain RGB images with output pixel size similar to that of high resolution input data.

2.3.5. Simple mean

The Simple Mean approach applies a simple mean averaging equation to each combination of Pansharpened imagery with one of the multispectral images. In this approach, the pansharpened image is obtained with the formula.

$$psh = \frac{pan + mul}{2} \quad (10)$$

where *Psh* is pansharpened image, *Pan* is the panchromatic image and *Mul* is the multispectral image (Belfiore et al., 2016). A detailed description of the pansharpening methods can be found in the ArcGIS version 10.2 software in-built user manual as well as online help facility (https://desktop.arcgis.com/en/arcmap/10.3/manage-data/raster-and-images/fundamentals-of-panchromatic-sharpening.htm).

2.4. Supervised LULC mapping

LULC mapping was done using the Support Vector Machines algorithm (Adelabu et al., 2013) and was followed by accuracy

assessment in the ENVI software. SVM fits an optimal separating hyperplane using two classes of training samples within a multidimensional feature space. It attempts to maximize the distance between the closest training samples (support vectors) and the hyperplane (Adelabu et al., 2013; Hsu et al., 2003). The vectors are projected into a high-dimensional feature space by means of a kernel and fitting of an optimal hyperplane to separate classes using an optimization function. In this study, we selected a Gausian radial basis kenel function since it is efficient in working in an infinite-dimensional space and has a single parameter (Adelabu et al., 2013; Melgani and Bruzzone, 2004). Throughout the study, default values of 0.083 and 100 were used for Gamma in kennel function and penalty parameter, respectively. The classification was followed by accuracy assessment which derived indicators from a confusion matrix. A confusion matrix depicts how pixels were classified in comparison to their actual LULC class observed in the field (ground truth). Accuracy indicators derived from the confusion matrix were Overall Accuracy (*OA*) and Kappa (*k*) (Sheykhmousa et al., 2020). According to Sheykhmousa et al. (2020), use of *OA* and *k* is the most common and reliable way of reporting accuracy. The indices were selected based on their popularity and wide adoption in literature. The classification was guided by 70% of the sample points per class obtained from the field while the remaining 30% were used for accuracy assessment. For each class, the points were split into training and accuracy assessment sets using R software using a stratified random sampling approach. Supervised classification using SVM algorithm and accuracy assessment were repeated using the pansharpened data from the methods described above. The first LULC map produced using the un-pansharpened 30m dataset was used as a control for comparison with the different pansharpening methods. Mapping accuracies were then compared between mapping data with and without pansharpening. Accuracies were also compared between the different pansharpening methods.

2.5. Effect of pansharpening on discriminability of LULC classes

Separability test was done using the Transformed Divergence Separability Index (TDSI) - (Chemura and Mutanga, 2017; Matongera et al., 2017) to determine the extent to which LULC types could be differentiated using input datasets (imagery and class samples). The TDSI ranges between 0 and 2; values close to 0 imply that the classes cannot be distinguished and should be merged to reduce spectral confusion while values close to 2 indicate that two LULC classes are easily distinguishable. The step is necessary to eliminate mapping errors due to spectral similarities between any two classes. High interclass separability indicates potential of the data to map LULC with high accuracy. Separability analysis was done to compare the capabilities of un-pansharpened and pansharpened data to discriminate LULC in the study area.

2.6. Retrieval of LST

A single channel approach using Band 10 of Landsat 8 was used to retrieve LST from thermal infrared data for the hot and dry season (Mushore et al., 2018). Mushore et al. (2018) indicated that the hot and dry season cover a period from mid-September to mid-November. Thermal infrared digital numbers were converted to brightness/blackbody temperature (using Landsat specific Planck curve) which was converted to LST after emissivity correction (Sobrino, 2004; Tran et al., 2017). Details of temperature retrieval steps are described in the sections below.

2.6.1. Conversion from digital numbers to radiances

The surface-leaving radiance was converted to apparent surface temperature using the Planck curve specific Landsat implementation;

$$\boldsymbol{L_I = M_I Q_{CAL} + A_L} \tag{11}$$

where L_l is Top of Atmosphere (TOA) spectral radiance (Watts/(m^2*srad*μm)) - (https://www.usgs.gov/landsat-missions/using-usgs-landsat-level-1-data-product), M_l is Band-specific multiplicative rescaling factor from the metadata (RADIANCE_MULT_BAND_x, where *x* is the band number), Q_{cal} is Quantized and calibrated standard product pixel values (DN) and A_L is Band-specific additive rescaling factor from the metadata (RADIANCE_ADD_BAND_x, where *x* is the band number). The coefficients are obtained from the metadata file accompanying each Landsat 8 data download as described in U.S. Geological Survey, (2019).

2.6.2. Conversion from radiances to brightness temperature

The steps for deriving LST were executed following Sobrino (2004). Initially, digital numbers of thermal data were converted to thermal radiances using equation (11). The computed radiances were used in Equation (12) to derive brightness/blackbody temperature.

$$\boldsymbol{T_B = \frac{K_2}{\ln\left(\frac{K_1}{L_{Thermal}} + 1\right)}} \tag{12}$$

where T_B is the at-satellite brightness temperature in degrees Kelvin, K_2 is the Band-specific thermal conversion constant from the metadata (K2_CONSTANT_BAND_x where *x* is the band number 10), K_1 is the Band-specific thermal conversion constant from the metadata (K1_CONSTANT_BAND_x where x is band number 10) and $L_{Thermal}$ is the product of the Radiance formula. Emissivity is assumed to be equal to 1 in order to retrieve brightness temperature over surfaces. However, this is not real for typical objects and computation of LST needs to take emissivity into account. Therefore, LST was calculated by applying emissivity correction on brightness temperature using Equation (13) (subtracting 273.15 converts units of temperature from Kelvins to Degrees Celsius)

$$T_S = \frac{T_B}{1 + \left(\frac{\lambda \times T_B}{\alpha}\right) \ln \varepsilon} - 273.15 \quad (13)$$

where T_S is the LST in Degree Celsius (Bakar et al., 2016). λi s the central wavelength of emitted radiance (10.9 μm for band 10 of Landsat 8), ε is the emissivity and α is a constant (1.438 × 10^{-2}mK). Emissivity was obtained from NDVI using Equation (15) (Mohamed et al., 2017; Van De Griend and Owe, 1993; J. Zhang et al., 2006);

$$\varepsilon = a + b \ln(NDVI) \quad (14)$$

where $a = 1.0094$ and $b = 0.047$. The equation was chosen due to ease of computation, parsimony and proven applicability in a tropical environment as it was developed in Botswana, which is close to the study area (Van De Griend and Owe, 1993). The equation was also found applicable to National Oceanic and Atmospheric Adminstration Advanced Very High Resolution Radiometer (NOAA AVHRR) and Landsat data while in this study, Landsat 8 data were used. The NDVI was retrieved using Equation (15) (Rasul et al., 2015; Tariq et al., 2020))

$$NDVI = \frac{(NIR - RED)}{(NIR + RED)} \quad (15)$$

where *NIR* and *RED* are the reflectances in the Near Infrared (Band 5) and Red (Band 4) of Landsat 8, respectively (U.S. Geological Survey, 2019).

In this study three image scenes (dates) within the hot season were used such that LST was computed for each overpass. This was necessary because (i) pansharpening requires a multi-layer file with at least three bands and (ii) better understanding of surface temperature spatial distribution in a season is better deduced as an average than using a single scene.

2.7. Quality assessment of pansharpening using LST, NDVI and UI

Data were extracted (using the "Extract by points" tool in ArcGIS software) from un-pansharpened and pansharpened LST, NDVI and UI from 300 randomly generated points fairly distributed across study area for quality assessment. The UI was calculated using equation (16) (Kawamura, 1996)

$$UI = \left(\frac{(Band7 - Band5)}{(Band7 + Band5)} + 1\right) \times 100 \quad (16)$$

Correlation Coefficient and RMSE were used to assess the accuracy of pansharpened against un-pansharpened retrievals. Correlation between un-pansharpened and pansharpened is one of the best methods to assess quality with high values (close to 1) for good spectral preservation (Ayhan and Atay, 2012; Palubinskas, 2015). Correlation also shows how much the quality of the original data is maintained while low RMSE would also indicate accuracy of the pansharpened data (Sarp, 2014). The smaller the RMSE the higher the correspondence between pansharpened and un-pansharpened data/retrieval (Johnson, 2014; Palubinskas, 2015; Xu et al., 2017). The quality assessments were performed to compare un-pansharpened with pansharpenpansharpened LST and vegetation indices (Normalized Difference Vegetation Index and Urban Index).

2.8. Linking LULC with LST

2.8.1. Qualitative link between LST and LULC before and after pansharpening

The retrieved un-pansharpened and pansharpened LST and LULCs were overlaid in ArcGIS version 10.2 software. The Zonal Statistics Tool in ArcGIS was used to compute average LST for each LULC class before and after pansharpening. The procedure was done using data with and without pansharpening for comparison purposes. This was done after identifying the pansharpening method which provided for the highest mapping accuracy. The purpose was to determine the extent to which mean LSTs per LULC differed between un-pansharpened and pansharpened retrievals. This also allowed for an investigation whether relationship between LULC and LST was changed by pansharpening.

2.8.2. Effect of pansharpening on the quantitative link between LULC and LST

In addition to assessment of link between qualitative LULC classes and LST, quantitative link between LST and NDVI as well as UI (as quantitative proxies for LULC) was executed. This was done to ascertain if pansharpening compromises the scale of invariance of

Table 2
Effects of pansharpening methods on mapping accuracy.

Method	Overall accuracy (%)	Kappa coefficient	Improvement in accuracy (%)
Un-pansharpened	89.77	0.80	–
Simple Mean	92.13	0.87	2.63
Intensity Hue Saturation	91.75	0.86	2.21
Esri	91.69	0.85	2.14
Brovey	90.59	0.84	0.91
Gram-Schmidt	89.45	0.82	−0.36

known spatial correlation between UI and LST as well as between NDVI and LST. The correlation was assessed before and after pansharpening by comparing the directions (slopes) and explained variance (r-squared) of regression equations. Difference between correlation before and after pansharpening shows extent to which quality is maintained (Sarp, 2014).

3. Results and discussion

3.1. Effects of pansharpening on LULC mapping accuracy

Despite the complexity of mapping urban landscape using moderate resolution remotely sensed data, OAs were more than 89% before and after pansharpening (Table 2). Based on OA, pansharpening using the Gram Schmidt method resulted in lower mapping accuracy than using data without pansharpening (un-pansharpened). Although the OA was lower, the kappa coefficient was higher than using un-pansharpened data. The Simple Mean pansharpening methods provided data with the highest classification accuracy (92.13%). In general, pansharpening resulted in higher classification accuracy by increasing either the OA, kappa or both indicators. Improvements in accuracy did not exceed 5% for all pansharpening methods. This could be because LULC such as built-up areas were occupying large areas and in most cases easily classified even at 30m resolution. Furthermore, in places where LULCs are heavily fragmented, the 15m resolution could still be inadequate to resolve the mixed pixel effect.

All the methods used for pansharpening improved the classification accuracy when compared to the use of the un-pansharpened 30m resolution Landsat 8 reflective data. The improvement in accuracy can be attributed to the improved resolution after pansharpening. At an improved 15m spatial resolution, the mixed pixel effect due to urban heterogeneity was reduced, hence better mapping accuracy. This finding is consistent with Gilbertson et al., (2017) who found that a pansharpened Landsat 8 data improved the classification accuracy by ~15% using Pixel Based Image Analysis (PBIA) and Object Based Image Analysis (OBIA) approaches in Western Cape, South Africa. Gilbertson et al., (2017) obtained at least 5% higher accuracies than in this study because herein LULC was mapped in an urban setting while they mapped in a less complex agricultural area. Another study by Sivanpillai and Miller (2008) in Wyoming, USA showed that pansharpening Landsat imagery maps small water bodies with higher accuracy than the traditional Landsat data, while Marangoz et al. (2006) indicated that LULC classes such as urban, water and agricultural areas were easily identified after pansharpening of Landsat and ASTER images. In this study, we have also shown that LULC classes are more separable using pansharpened than un-pansharpened data.

Pansharpening using Simple Mean method provided the highest classification accuracy compared to Gram-Schmidt, Esri, Brovey and IHS. The sequence of superiority in this study was Simple Mean, Intensity Hue Separation, ESRI method, Brovey and then Gram Schmidt, respectively. Similar to Ayhan & Atay (2012), Intensity Hue Separation performed better than Brovey while Gram Schmidt had the lowest classification Overall Accuracy. We attribute the observed sequence in superiority of performance to differences in suitability of the methods in the study area. Previous studies (Ayhan and Atay, 2012; Jawak and Luis, 2013; Sarp, 2014; Xu et al., 2014, 2017) have demonstrated that different methods are best suited for different regions, hence we found that Simple Mean is best for Bulawayo Metropolitan City for daytime data during a short period. This is demonstrated by the accuracy in LULC mapping as well as high correlation between un-pansharpened and sharpened LST and vegetation indices. Overall, the findings confirm notion by Omran (2012) that resolution affects classification accuracy and detection of changes in land features.

3.2. Effect of pansharpening on inter-class separability

Transformed Divergence Separability Index (TDSI) values obtained from the separability test were between 1 and 2 before and after un-pansharpened (Table 3). The TDSI values were higher after than before pansharpening, indicating that the process increased discriminability of LULC classes. For example, TDSI between Densely built-up and Low density residential areas were 1.327 and 1.647 before and after pansharpening, respectively. Pansharpening did not affect the order from least to most separable classes, however, it increased discriminability of any two LULC classes. As such, Built-up and Low density were the least separable (TDSI<1.65). The Built-

Table 3
LULC Separability values following Simple Mean based pansharpening.

LULC Classes	Separability value (TDSI)	
	Un-pansharpened	pansharpened
Densely built-up – L-M density	1.327	1.647
Dense forest – L-M density	1.398	1.699
Water body – L-M density	1.403	1.701
Dense forest - Bare area	1.426	1.714
L-M density - Bare area	1.497	1.875
Grassland – L-M density	1.563	1.896
Dense forest - Water body	1.599	1.897
Densely built-up - Water body	1.611	1.920
Dense forest – Grassland	1.679	1.945
Grassland - Bare area	1.690	1.945
Water body - Bare area	1.730	1.988
Densely built-up - Dense forest	1.777	1.993
Densely built-up – Grassland	1.801	1.999
Average	1.577	1.863

*L-M – Low – medium density residential including sparse forest.

up and grassland were the most separable with and without pansharpening (TDSI>1.8). Pansharpening reduces the mixed pixel effect and increase separability of any two LULC classes hence the increase in mapping accuracy.

3.3. Comparison of pansharpened with un-pansharpened image-based indices and LST

Table 4 shows the correlation between un-pansharpened and pansharpened LST and vegetation indices. RMSEs were also low and close to zero for Normalized Difference Vegetation Index and Urban Index. On the other hand, correlation between un-pansharpened and sharpened LST was high compared to that of LST with vegetation indices.

3.4. LULC map for Bulawayo metropolitan city

A casual visual inspection shows a general agreement in the mapped distribution of classes using data before (Fig. 2a) and after pansharpening (Fig. 2b). For example, the bare areas, which dominated the western parts of the city and the densely built-up central to southern area were captured on both maps. Both maps depicted that low density residential areas occupied the western parts of the city. Differences were observed in the level of detail between the two maps. The boxed areas in Fig. 2 show the differences noted between the two maps and that without pansharpening, LULC classes were generalized in some places. There were places which were assigned to different classes in the two maps. A closer look at the north most highlight box shows areas which were classified as dense forest before pansharpening but classified as bare after pansharpening. Some classes within classes that were not detected without pansharpening were observed on map produced after pansharpening. The small differences were attributed to dissimilarity in mapping accuracy between classification based on un-pansharpened and that derived from pansharpened data. The highly accurate map derived from pansharpened data also showed small LULC fragments which were missing when classification was based on original data resolution. Increased surface heterogeneity and LULC fragmentation of natural and pre-existing LULC typical of expanding city was better depicted after pansharpening as the original dataset merged small fragments with surrounding large LULC patches (see southernmost box). The typical fragmentation of non-built LULC types and conglomeration of densely built-up areas was better displayed after than before pansharpening.

The findings from this study agree with that pansharpening allows finer details to be visualized and enhances image segmentation and classification accuracy (Gilbertson et al., 2017a; He et al., 2014; Johnson, 2014). This proves that the lack in spatial details of un-pansharpened multispectral data can be augmented by improvements from data fusion. In this study for instance, some of the spatial details that were missing on both LULC and LST data were revealed after pansharpening, implying that fused data captured variations in thermal radiance (Weng et al., 2007). Mallick et al. (2013), using 10 m resolution Advanced Thermal and Land Assessment Sensor data, also found that high resolution data improved assessment of LST derivatives in complex landscapes. Improved accuracy and correlation between LULC and LST in this study implies that pansharpening reduced the mixed pixel problem and made remotely sensed retrieval to better represent field observations than without pansharpening (Chrysoulakis, 2003; Prigent et al., 2003). There were also similarities between un-pansharpened and pansharpened retrievals. This could correspond to areas where LULC with similar characteristics stretched over large spatial extents, resulting in homogeneous thermal conditions (Weng et al., 2007). In addition to benefits from improved spatial resolution, the procedure was also cost effective, fast and easy which characterizes component substitution pansharpening methods (Aiazzi et al., 2007; He et al., 2014; Johnson, 2014).

Table 5 shows areas covered by each class with and without pansharpening with bare surface covering more spatial extent after than before pansharpening. The rest of the classes covered more area before than after pansharpening. Dense forest area decreased to approximately 50% of the area before pansharpening. Evidently, for all classes, allocation was different with and without pansharpening. The differences in areas were attributed to the enhanced capabilities of pansharpened data to identify and map LULCs with higher accuracy than un-pansharpened data. Increase in spatial resolution enables description of small features (Liu and Weng, 2009) thus enhancing mapping capabilities, hence the changes in LULC distribution obtained after pansharpening.

3.5. Effect of pansharpening on LST spatial structure

Fig. 3 shows that without pansharpening, there is smoothing, which reduces the number of patches of a given range. There were a large number of small patches (increased fragmentation) after pansharpening, while most locations were placed into the same LST categories as before pansharpening. Other temperature details missed in the un-pansharpened map were observed on the pansharpened map. For example, the south western boxes in Fig. 3b indicate areas with low temperature (below 32 °C), which were missing before pansharpening in Fig. 3a. These areas with slightly low temperature coincided with low density residential and dense vegetation areas. Before pansharpening, at a resampled spatial resolution of 30m, the proportion covered by the above 32 °C LST category occupied a larger area than after pansharpening. Pansharpening increases the capability to discern small temperature spatial details in space. Overall, temperature categories of small spatial extent are better captured after than before pansharpening. This concurs with the observation that high spatial resolution data can discriminate the thermal responses of individual components of a specific surface type (Voogt, 2000).

Table 4
Accuracy of pansharpened LST and Vegetation Indices.

Quantity	Correlation coefficient	RMSE
Normalized Difference Vegetation Index	0.940	0.023
Urban Index	0.944	0.032
LST	0.976	0.998 (°C)

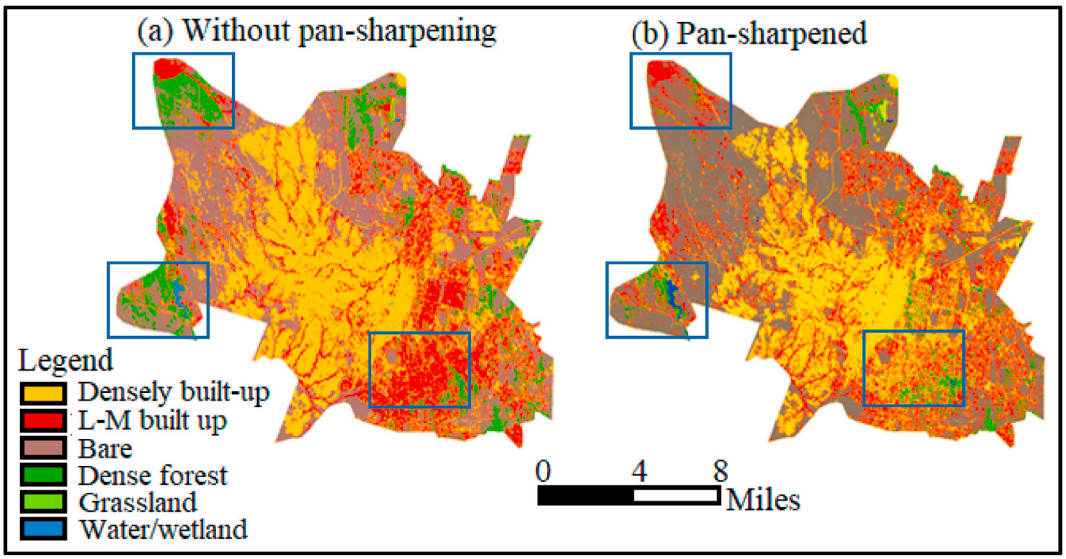

Fig. 2. LULC classes before and after pansharpening (*L–M: Low to medium density).

Table 5
Area for each LULC class before and after pansharpening.

LULC class	Area (hectares)	
	Pansharpened	Un-pansharpened
Bare	7752	4432
Densely built-up	11224	15770
Dense forest	1409	2147
Low-Medium built-up/Sparse forest	2480	4395
Grassland	272	409
Water	119	203

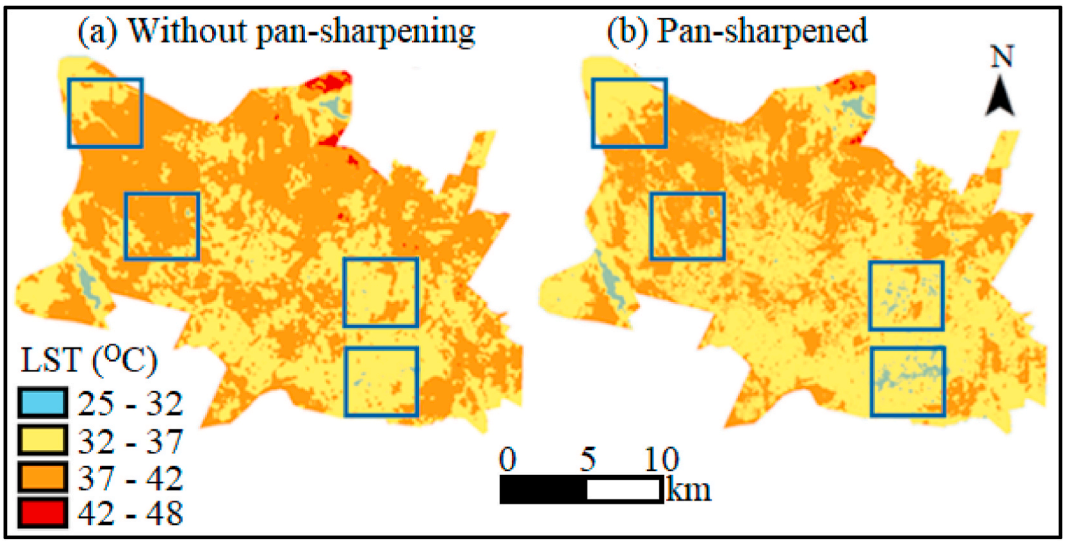

Fig. 3. Temperatures before and after pansharpening.

Panchromatic sharpening increases the spatial resolution and provides a better visualization of a multi-band image using the high-resolution, single-band image (Rahaman et al., 2017). This agrees with the finding that LSTs derived from pansharpened thermal infrared data showed detailed and localized temperature variations missing in analysis before pansharpening. LST characterization

was also improved by pansharpening evidenced by the ability to indicate low temperatures in areas with low density of building and forest better than before pansharpening. This was further supported by the high Correlation Coefficient between LST and vegetation indices after pansharpening. The effect of fragmentation depicted by LULC map was better captured by the corresponding responses of LST after pansharpening. Before pansharpening, the 30m resolution LST maps depicted broad classes, significant generalization and missing details. High correlation and low RMSE between un-pansharpened and pansharpened LST indicated high accuracy and that the quality of LST maps were maintained (Ayhan and Atay, 2012; Sarp, 2014). Although there were no field temperature measurements to assess accuracy of pixel values, we believed that LSTs derived from pansharpened data were more accurate than without pansharpening, due to a slight increase in correlation between LST and Urban Index after pansharpening. Therefore, the resolution of thermal data was improved without compromising retrievals from the new dataset after fusion.

3.6. Link between LULC and LST

Pansharpened mean LSTs did not significantly differ with mean un-pansharpened LSTs for the different LULC types. The average LST for the whole area was slightly higher before (35.0 °C) than after pansharpening (34.7 °C). Except for the Forest class, where the difference was 1 °C, the mean temperature for other LULC types after pansharpening was at most 0.1 °C lower than when LST was derived from un-pansharpened thermal data (Fig. 4). Slightly higher LSTs can be due to that spatial variability is increased, also because of the fine scale details that are derived from pansharpened data. The average LST changed from 39.1 to 39 °C for bare areas and 37.8 to 37.7 °C for densely built-up areas while it remained at 37.1 °C for low to medium density residential areas. Pansharpening did not affect the relationship between LST and LULC. For example, highest LSTs were recorded on bare and densely built-up areas for both un-pansharpened and pansharpened data (Fig. 4). Lowest LSTs were recorded on water bodies and forests, respectively, before and after pansharpening. Low LSTs were also recorded on grasslands while bare areas (warmest) and densely built-up areas had high LSTs. Low-medium density residential areas recorded slightly lower LSTs than densely built-up areas (difference less than 1 °C).

Although pansharpening improved mapping quality, it did not affect the known relationship between LULC types and LST. As expected, highest temperatures were recorded in bare and built-up areas with and without pansharpening. This is consistent with established knowledge that bare, impervious and built surfaces have higher solar absorption and a greater thermal conductivity (Srivanit et al., 2012). Highest LST in bare areas compared to other LULC could be due to combined effect of absence of healthy vegetation and low water table (during hot and dry season). Absence of vegetation water and abundance of dry surfaces reduced the cooling effect of latent heat transfer resulting in high LST over bare areas. In both pansharpened and un-pansharpened datasets, dense forest, grassland and water areas recorded low temperature due to the cooling effect of evaporation. In consistency with Kayet et al. (2016), the heat mitigation value of vegetation as observed over agricultural cropland, dense vegetation (forest), and sparse vegetation (grass/park) land use categories was observed in this study. Urbanization migrates pixels from cool to hot conditions while surface wetness increases heat capacity and heat transfer through latent heat causing low temperatures over vegetation and water surfaces (Amiri et al., 2009). In Harare, Zimbabwe, Mushore et al. (2017) also showed that vegetation abundance has heat mitigation value while dense buildings and impervious surfaces cause temperature elevation. Jiang and Tian (2010) showed that the changes of vegetation cover to imperviousness and built-up increases LST. Evidently, pansharpening the two datasets to the same resolution is a great step in overcoming this mismatch without affecting known relationships. While awaiting the outcome of sensor development efforts on high resolution thermal data, pansharpening can be used to improve urban vegetation and thermal mapping. The use of freely available dataset like the Landsat series is particularly valuable for resource constrained nations and non-funded studies that cannot afford high resolution datasets.

The percentage of variance in LST explained by UI was almost similar before and after pansharpening (negligible increase in R-squared value). Pansharpened LST maintained a positive correlation with Urban Index, implying that the procedure did not weaken

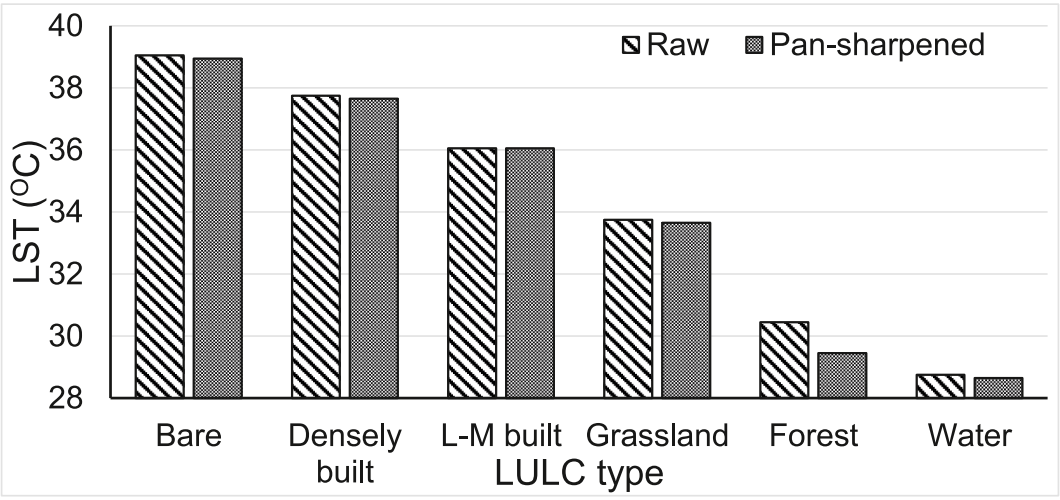

Fig. 4. Mean LST per class before and after pansharpening.

spatial correlation between LULC types. A closer look at the scatter diagrams in Fig. 5a and Fig. 5b show that the values are different at some of the points, indicating that the spatial configuration of LSTs changed after sharpening. Similarity in correlation before and after pandsharpening indicates that the procedure increased spatial resolution without compromising the quality of the data (Sarp, 2014).

Similar to UI, caused a very slight change in the correlation between NDVI and LST (Fig. 6). The minor improvement in the correlation was attributed to effect of pansharpening in aligning LST pixels to the actual land surface characteristics causing the LST variations. Improved accuracy and correlation between LULC and LST in this study implies that pansharpening reduced the mixed pixel problem and made remotely sensed retrieval to better represent field observations than without pansharpening (Chrysoulakis, 2003; Prigent et al., 2003). There were also similarities between un-pansharped and pansharpened retrievals. This could correspond to areas where LULC with similar characteristics stretched over large spatial extents, resulting in homogeneous thermal conditions (Weng et al., 2007). In addition to benefits from improved spatial resolution, the procedure was also cost effective, fast and easy which, characterizes component substitution pansharpening methods (Aiazzi et al., 2007; He et al., 2014; Johnson, 2014).

4. Conclusions and perspectives

It is however recommended that further studies should be done in other seasons, especially the cool and rainy season to assess effect of seasonality on pansharpening retrievals. This study focused on pansharpening methods engraved in ArcGIS environment which may blind researchers on the value of other methods for similar tasks. It is thus necessary to test other pansharpening methods to determine those best suited for LULC mapping and temperature characterization in urban landscapes. Due to absence of in–situ surface temperature measurements, remotely sensed LST retrievals were not validated. This made it difficult to adequately ascertain the effect of pansharpening on accuracy of LST pixel values. Therefore, there is need to coincide LST observations with Landsat 8 overpass to improve remotely sensed retrievals and pansharpening comparisons. Sensor development and measurement techniques should consider availing high temporal resolution data (such as at 10 min intervals) to allow analysis of rapidly changing surface thermal phenomena. Similarly, sensor development efforts should strive to come up with a mission which provides thermal data with adequate spatial resolution (such as >10m) to reliably map urban surface temperature variations.

Based on findings, we concluded that due to improved spectral and radiometric qualities of Landsat 8 data, LULC accuracy was high (89.77%) even before pansharpening (at 30m resolution). Compared to four other tested methods, Simple Mean pansharpening technique was superior in accuracy (92.13%) and in pronouncing spatial details. Pansharpening (to 15m resolution) increased discriminability (TDSI between 1.647 and 1.999 compared to between 1.327 and 1.777 and mapping accuracy of land covers and LST in a complex urban setting. It produced LULC and LST maps with fine details, which were missed at 30 m resolution of un-pansharpened data, respectively. As such after pansharpening small details such as LSTs in the 25–32 °C ranges could be seen withing the 32–37 °C areas contrary to limited information in un-pansharpened data. LSTs were slightly lower after than before pansharpening (by at most 1 °C), however, both maps depicted similar trends and high correlation ($r > 0.94$). Although pansharpening improved details and accuracy, it did not compromise the known relationships and correlations between LULC, vegetation indices and LST. As a result, highest LSTs were recorded in dry bare areas (39.1 and 39 °C) while lowest LSTs were recorded in water areas (28.8 and 28.7 °C) before and after pansharpening. Furthermore, it increased correlation between LST and NDVI (from 0.4574 to 0.4665) and between LST and UI (from 0.619 to 0.6442). Overall, the study concludes that pansharpening serves as a cost effective way to improve spatial resolution of thermal data and solve the problem of mismatch in resolution between Landsat 8 derived LULC and LST, valuable while awaiting higher resolution sensor developments outcomes.

Author credit

Dr Terence Mushore developed the concept, reviewed literature, collected data, performed analysis, did the write up of the manuscript at all stages of development. Prof Mutanga and Prof Odindi were involved in all parts from conceptualization to improvement of the quality of the manuscript as well as providing overall guidance through their supervisory role. Prof Dube participated in data analysis and preparation of draft manuscript while Vanessa Sadza was part of the field data collection team and contributed in the analysis and drafting of manuscript.

Ethics

All ethical issues including crediting sources of information were followed in this research.

Data availability

Availability of data	Template for data availability statement	Policy
Data derived from public domain resources	The data that support the findings of this study are available in United States Geological Survey's (USGS) earth explorer website at https://earthexplorer.usgs.gov/. These data were derived from the following resources available in the public domain: https://earthexplorer.usgs.gov/https://fairsharing.org/bsg-d001522	All

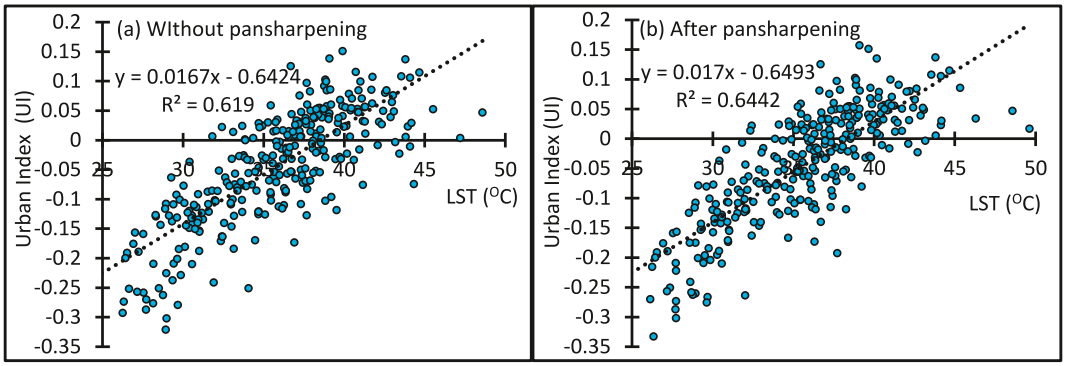

Fig. 5. Response of correlation between LST and Urban Index to pansharpening.

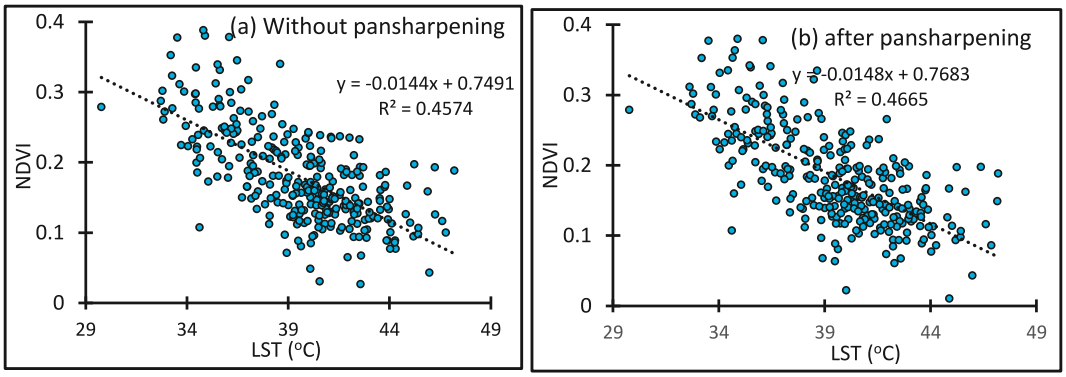

Fig. 6. Effect of pansharpening on the correlation between LST and NDVI.

Declaration of competing interest

The authors declare that they have no known competing financial interests or personal relationships that could have appeared to influence the work reported in this paper.

Acknowledgements

We acknowledge the National Research Foundation (NRF) of South Africa and the Germany DAAD climapAfrica for funding the research, This work was funded by the National Research Foundation of South Africa (NRF) Research Chair in Land Use Planning and Management (Grant Number: 84157), The research of this article was supported by DAAD within the framework of the climapAfrica programme with funds of the Federal Ministry of Education and Research. The publisher is fully responsible for the content.

References

Acharya, T.D., Yang, I., 2015. Exploring landsat 8. Int. J. IT Eng. Appl. Sci. Res. (IJIEASR) 4 (4), 4–10.

Adelabu, S., Mutanga, O., Adam, E., Cho, M.A., 2013. Exploiting machine learning algorithms for tree species classification in a semiarid woodland using RapidEye image. J. Appl. Remote Sens. 7 (1), 073480 https://doi.org/10.1117/1.jrs.7.073480.

Agam, N., Kustas, W.P., Anderson, M.C., Li, F., Neale, C.M.U., 2007. A vegetation index based technique for spatial sharpening of thermal imagery. Remote Sens. Environ. 107 (4), 545–558. https://doi.org/10.1016/j.rse.2006.10.006.

Aiazzi, B., Baronti, S., Selva, M., 2007. Improving component substitution pansharpening through multivariate regression of MS+Pan data. IEEE Trans. Geosci. Rem. Sens. 45 (10), 3230–3239. https://doi.org/10.1109/TGRS.2007.901007.

Amiri, R., Weng, Q., Alimohammadi, A., Alavipanah, S.K., 2009. Spatial-temporal dynamics of land surface temperature in relation to fractional vegetation cover and land use/cover in the Tabriz urban area, Iran. Remote Sens. Environ. 113 (12), 2606–2617. https://doi.org/10.1016/j.rse.2009.07.021.

Arif, F., Akbar, M., 2005. Resampling air borne sensed data using bilinear interpolation algorithm. In: Proceedings of the 2005 IEEE International Conference on Mechatronics. ICM, pp. 62–65. https://doi.org/10.1109/ICMECH.2005.1529228, 05, 2005.

As-syakur, A.R., Adnyana, I.W.S., Arthana, I.W., Nuarsa, I.W., 2012. Enhanced built-UP and bareness index (EBBI) for mapping built-UP and bare land in an urban area. Rem. Sens. 4 (10), 2957–2970. https://doi.org/10.3390/rs4102957.

Ayhan, E., Atay, G., 2012. Spectral and spatial quality analysis in pansharpening process. J. Indian Soc. Remote Sens. 40 (3), 379–388. https://doi.org/10.1007/s12524-011-0185-0.

Bai, Y., Wong, M.S., Shi, W.Z., Wu, L.X., Qin, K., 2015. Advancing of land surface temperature retrieval using extreme learning machine and spatio-temporal adaptive data fusion algorithm. Rem. Sens. 7 (4), 4424–4441. https://doi.org/10.3390/rs70404424.

Bakar, S.B.A., Pradhan, B., Lay, U.S., Abdullahi, S., 2016. Spatial assessment of land surface temperature and land use/land cover in Langkawi Island. IOP Conf. Ser. Earth Environ. Sci. 37 (1) https://doi.org/10.1088/1755-1315/37/1/012064.

Belfiore, O.R., Meneghini, C., Parente, C., Santamaria, R., 2016. Application of different pansharpening methods on worldview-3 images. ARPN J. Eng. Appl. Sci. 11 (1), 490–496.
Bhandari, A.K., Kumar, A., Singh, G.K., 2012. Feature extraction using normalized difference vegetation index (NDVI): a case study of jabalpur city. Proc. Technol. 6, 612–621. https://doi.org/10.1016/j.protcy.2012.10.074.
Buyantuyev, A., Wu, J., Gries, C., 2007. Estimating vegetation cover in an urban environment based on Landsat ETM+ imagery: a case study in Phoenix, USA. Int. J. Rem. Sens. 28 (2), 269–291. https://doi.org/10.1080/01431160600658149.
Chemura, A., Mutanga, O., 2017. Developing detailed age-specific thematic maps for coffee (Coffea arabica L.) in heterogeneous agricultural landscapes using random forests applied on Landsat 8 multispectral sensor. Geocarto Int. 32 (7), 759–776. https://doi.org/10.1080/10106049.2016.1178812.
Chen, X.L., Zhao, H.M., Li, P.X., Yin, Z.Y., 2006. Remote sensing image-based analysis of the relationship between urban heat island and land use/cover changes. Remote Sens. Environ. 104 (2), 133–146. https://doi.org/10.1016/j.rse.2005.11.016.
Choi, M., Kim, H.H., Cho, N., 2006. An improved intensity-hue-saturation method for IKONOS image fusion. Pan 1–10, 00(00). http://scholar.google.com/scholar?hl=en&btnG=Search&q=intitle:An+improved+intensity-hue-saturation+method+for+IKONOS+image+fusion#0%5Cnhttp://citeseerx.ist.psu.edu/viewdoc/download?doi=10.1.1.97, 7467&rep=rep1&type=pdf.
Chrysoulakis, N., 2003. Estimation of the all-wave urban surface radiation balance by use of ASTER multispectral imagery and in situ spatial data. J. Geophys. Res. Atmos. 108 (18), 1–10. https://doi.org/10.1029/2003jd003396.
Dube, Timothy, et al., 2016. Quantifying aboveground biomass in African environments: A review of the trade-offs between sensor estimation accuracy and costs. Trop. Ecol. 57 (3), 393–405.
Gilbertson, J.K., Kemp, J., van Niekerk, A., 2017a. Effect of pansharpening multi-temporal Landsat 8 imagery for crop type differentiation using different classification techniques. Comput. Electron. Agric. 134, 151–159. https://doi.org/10.1016/j.compag.2016.12.006.
Gilbertson, J.K., Kemp, J., van Niekerk, A., 2017b. Effect of pansharpening multi-temporal Landsat 8 imagery for crop type differentiation using different classification techniques. Comput. Electron. Agric. 134, 151–159. https://doi.org/10.1016/j.compag.2016.12.006.
Goldreich, Y., 2006. Ground and top of canopy layer urban heat island partitioning on an airborne image. Remote Sens. Environ. 104 (2), 247–255. https://doi.org/10.1016/j.rse.2005.08.018.
Gumbo, B., Mlilo, S., Broome, J., Lumbroso, D., 2003. Industrial water demand management and cleaner production potential: a case of three industries in Bulawayo, Zimbabwe. Phys. Chem. Earth 28 (20–27), 797–804. https://doi.org/10.1016/j.pce.2003.08.026.
Gusso, A., Bordin, F., Veronez, M., Cafruni, C., Lenz, L., Crija, S., 2014. Multitemporal Analysis of Thermal Distribution Characteristics for Urban Heat Islands Management. 4th WOrld Sustainability Forum. https://doi.org/10.3390/wsf-4-f009 f009.
He, X., Condat, L., Bioucas-Dias, J.M., Chanussot, J., Xia, J., 2014. A new pansharpening method based on spatial and spectral sparsity priors. IEEE Trans. Image Process. 23 (9), 4160–4174. https://doi.org/10.1109/TIP.2014.2333661.
Herold, M., Scepan, J., Clarke, K.C., 2002. The use of remote sensing and landscape metrics to describe structures and changes in urban land uses. Environ. Plann. 34 (8), 1443–1458. https://doi.org/10.1068/a3496.
Hsu, C.-W., Chang, C.-C., Lin, C.-J., 2003. A Practical Guide to Support Vector Classification. Taipei, Taiwan.
Huang, W., Xiao, L., Wei, Z., Liu, H., Tang, S., 2015. A new pansharpening method with deep neural networks. Geosci. Rem. Sens. Lett. IEEE 12 (5), 1037–1041. https://doi.org/10.1109/LGRS.2014.2376034.
Jawak, S.D., Luis, A.J., 2013. Improved land cover mapping using high resolution multiangle 8-band WorldView-2 satellite remote sensing data. J. Appl. Remote Sens. 7 (1), 073573 https://doi.org/10.1117/1.jrs.7.073573.
Jiang, J., Tian, G., 2010. Analysis of the impact of land use/land cover change on land surface temperature with remote sensing. Proc. Environ. Sci. 2 (5), 571–575. https://doi.org/10.1016/j.proenv.2010.10.062.
Johnson, B., 2014. Effects of pansharpening on vegetation indices. ISPRS Int. J. Geo-Inf. 3 (2), 507–522. https://doi.org/10.3390/ijgi3020507.
Kato, S., Matsunaga, T., Yamaguchi, Y., 2010. Influence of shade on surface temperature in an urban area estimated by ASTER data. Int. Arch. Photogram. Remote Sens. Spatial Inf. Sci. ISPRS Arch. 38, 925–929, 1995.
Kawamura, M., 1996. Relation between social and environmental conditions in Colombo Sri Lanka and the urban index estimated by satellite remote sensing data. In: Proc. 51st Annual Conference of the Japan Society of Civil Engineers, pp. 190–191.
Kawamura, M., Jayamanna, S., Tsujiko, Y., Sugiyama, A., 1998. Comparison of urbanization of four asian cities using satellite data. Dob. Gakkai Ronbunshu (608), 97–105. https://doi.org/10.2208/jscej.1998.608_97, 1998.
Kayet, N., Pathak, K., Chakrabarty, A., Sahoo, S., 2016. Spatial impact of land use/land cover change on surface temperature distribution in Saranda Forest, Jharkhand. Model. Earth Sys. Environ. 2 (3), 127. https://doi.org/10.1007/s40808-016-0159-x.
Liu, H., Weng, Q., 2009. Scaling effect on the relationship between landscape pattern and land surface temperature: a case study of Indianapolis, United States. Photogramm. Eng. Rem. Sens. 75 (3), 291–304. https://doi.org/10.14358/PERS.75.3.291.
Mallick, J., 2014. Land characterization analysis of surface temperature of semi-arid mountainous city Abha, Saudi Arabia using remote sensing and GIS. J. Geogr. Inf. Syst. 664–676. https://doi.org/10.4236/jgis.2014.66055, 06(06).
Mallick, J., Rahman, A., Singh, C.K., 2013. Modeling urban heat islands in heterogeneous land surface and its correlation with impervious surface area by using night-time ASTER satellite data in highly urbanizing city, Delhi-India. Adv. Space Res. 52 (4), 639–655. https://doi.org/10.1016/j.asr.2013.04.025.
Marangoz, A.M., Karakış, S., Oruç, M., 2006. Analysis of Object-Oriented Classification Results Derived from PansharpenPansharpened Landsat 7 Etm + and Aster Images. ASPRS, Ankara Workshop.
Matongera, T.N., Mutanga, O., Dube, T., Sibanda, M., 2017. Detection and mapping the spatial distribution of bracken fern weeds using the Landsat 8 OLI new generation sensor. Int. J. Appl. Earth Obs. Geoinf. 57, 93–103. https://doi.org/10.1016/j.jag.2016.12.006.
Melgani, F., Bruzzone, L., 2004. Classification of hyperspectral remote sensing images with support vector machines. IEEE Trans. Geosci. Rem. Sens. 42 (8), 1778–1790.
Mohamed, A.A., Odindi, J., Mutanga, O., 2017. Land surface temperature and emissivity estimation for Urban Heat Island assessment using medium- and low-resolution space-borne sensors: a review. Geocarto Int. 32 (4), 455–470. https://doi.org/10.1080/10106049.2016.1155657.
Muchingami, I., Hlatywayo, D.J., Nel, J.M., Chuma, C., 2012. Electrical resistivity survey for groundwater investigations and shallow subsurface evaluation of the basaltic-greenstone formation of the urban Bulawayo aquifer. Phys. Chem. Earth 50–52, 44–51. https://doi.org/10.1016/j.pce.2012.08.014.
Mushore, Terence D., Mutanga, O., Odindi, J., Dube, T., 2018. Determining extreme heat vulnerability of Harare Metropolitan City using multispectral remote sensing and socio-economic data. Spatial Sci. 63 (1), 173–191. https://doi.org/10.1080/14498596.2017.1290558.
Mushore, Terence Darlington, Mutanga, O., Odindi, J., Dube, T., 2017a. Assessing the potential of integrated Landsat 8 thermal bands, with the traditional reflective bands and derived vegetation indices in classifying urban landscapes. Geocarto Int. 32 (8), 886–899. https://doi.org/10.1080/10106049.2016.1188168.
Mushore, Terence Darlington, Odindi, J., Dube, T., Mutanga, O., 2017b. Prediction of future urban surface temperatures using medium resolution satellite data in Harare metropolitan city, Zimbabwe. Build. Environ. 122, 397–410. https://doi.org/10.1016/j.buildenv.2017.06.033.
Mutengu, S., Hoko, Z., Makoni, F.S., 2007. An assessment of the public health hazard potential of wastewater reuse for crop production. A case of Bulawayo city, Zimbabwe. Phys. Chem. Earth 32 (15–18), 1195–1203. https://doi.org/10.1016/j.pce.2007.07.019.
Omran, E.-S.E., 2012. Detection of land-use and surface temperature change at different resolutions. J. Geogr. Inf. Syst. 189–203. https://doi.org/10.4236/jgis.2012.43024, 04(03).
Owen, T.W., Carlson, T.N., Gillies, R.R., 1998. An assessment of satellite remotely-sensed land cover parameters in quantitatively describing the climatic effect of urbanization. Int. J. Rem. Sens. 19 (9), 1663–1681. https://doi.org/10.1080/014311698215171.
Palubinskas, G., 2015. Joint quality measure for evaluation of pansharpening accuracy. Rem. Sens. 7 (7), 9292–9310. https://doi.org/10.3390/rs70709292.
Parente, C., Santamaria, R., 2014. Synthetic sensor of landsat 7 ETM+ imagery to compare and evaluate pan-sharpening methods. Sensor. Transducers 177 (8), 294.
Prigent, C., Aires, F., Rossow, W.B., 2003. Land surface skin temperatures from a combined analysis of microwave and infrared satellite observations for an all-weather evaluation of the differences between air and skin temperatures. J. Geophys. Res. Atmos. 108 (10), 1–14. https://doi.org/10.1029/2002jd002301.

Rahaman, K.R., Hassan, Q.K., Ahmed, M.R., 2017. Pansharpening of landsat-8 images and its application in calculating vegetation greenness and canopy water contents. ISPRS Int. J. Geo-Inf. 6 (6), 168. https://doi.org/10.3390/ijgi6060168.

Rasul, A., Balzter, H., Smith, C., 2015. Spatial variation of the daytime surface urban cool island during the dry season in Erbil, Iraqi Kurdistan, from landsat 8. Urban Clim. 14, 176–186. https://doi.org/10.1016/j.uclim.2015.09.001.

Roy, D.P., Wulder, M.A., Loveland, T.R., Woodcock, C.E., Allen, R.G., Anderson, M.C., Helder, D., Irons, J.R., Johnson, D.M., Kennedy, R., 2014. Landsat-8: science and product vision for terrestrial global change research. Remote Sens. Environ. 145, 154–172.

Saaroni, H., Ben-Dor, E., Bitan, A., Potchter, O., 2000. Spatial distribution and microscale characteristics of the urban heat island in Tel-Aviv, Israel. Landsc. Urban Plann. 48 (1–2), 1–18. https://doi.org/10.1016/S0169-2046(99)00075-4.

Sarp, G., 2014. Spectral and spatial quality analysis of pansharpening algorithms: a case study in Istanbul. Eur. J. Rem. Sens. 47 (1), 19–28. https://doi.org/10.5721/EuJRS20144702.

Sekertekin, A., Abdikan, S., Marangoz, A.M., 2018. The acquisition of impervious surface area from LANDSAT 8 satellite sensor data using urban indices: a comparative analysis. Environ. Monit. Assess. 190 (7), 1–13. https://doi.org/10.1007/s10661-018-6767-3.

Shakya, N., Yamaguchi, Y., 2010. Vegetation, water and thermal stress index for study of drought in Nepal and central northeastern India. Int. J. Rem. Sens. 31 (4), 903–912. https://doi.org/10.1080/01431160902902617.

Sheykhmousa, M., Mahdianpari, M., Ghanbari, H., 2020. Support vector machine vs . Random forest for remote sensing image classification : a meta-analysis and systematic review. IEEE J. Sel. Top. Appl. Earth Obs. Rem. Sens. https://doi.org/10.1109/JSTARS.2020.3026724.

Shi, T., Huang, Y., Wang, H., Shi, C.E., Yang, Y.J., 2015. Influence of urbanization on the thermal environment of meteorological station: satellite-observed evidence. Adv. Clim. Change Res. 6 (1), 7–15. https://doi.org/10.1016/j.accre.2015.07.001.

Sivanpillai, R., Miller, S.N., 2008. Benefits of pan-sharpened Landsat imagery for mapping small waterbodies in the Powder River Basin, Wyoming, USA. Lakes & Reservoirs: Research & Management 13 (1), 69–76.

Sobrino, et al., 2004. Land surface temperature retrieval from LANDSAT TM 5. Remote Sensing of environment 90 (4), 434–440.

Srivanit, M., Hokao, K., Phonekeo, V., 2012. Assessing the impact of urbanization on urban thermal environment: a case study of bangkok metropolitan. Int. J. Appl. Sci. Technol. 2 (7), 243–256. http://www.ijastnet.com/journals/Vol_2_No_7_August_2012/26.pdf.

Stathakis, D., Perakis, K., Savin, I., 2012. Efficient segmentation of urban areas by the VIBI. Int. J. Rem. Sens. 33 (20), 6361–6377. https://doi.org/10.1080/01431161.2012.687842.

Tariq, A., Riaz, I., Ahmad, Z., Yang, B., Amin, M., Kausar, R., Andleeb, S., Farooqi, M.A., Rafiq, M., 2020. Land surface temperature relation with normalized satellite indices for the estimation of spatio-temporal trends in temperature among various land use land cover classes of an arid Potohar region using Landsat data. Environ. Earth Sci. 79 (1), 1–15. https://doi.org/10.1007/s12665-019-8766-2.

Tran, D.X., Pla, F., Latorre-Carmona, P., Myint, S.W., Caetano, M., Kieu, H.V., 2017. Characterizing the relationship between land use land cover change and land surface temperature. ISPRS J. Photogrammetry Remote Sens. 124, 119–132. https://doi.org/10.1016/j.isprsjprs.2017.01.001.

Tu, T.M., Huang, P.S., Hung, C.L., Chang, C.P., 2004. A fast intensity-hue-saturation fusion technique with spectral adjustment for IKONOS imagery. Geosci. Rem. Sens. Lett. IEEE 1 (4), 309–312. https://doi.org/10.1109/LGRS.2004.834804.

Tucker, C.J., 1979. Remote sensing of leaf water content in the near infrared. Remote Sens. Environ. 10, 23–32.

U.S. Geological Survey, 2019. Landsat 8 data users handbook. Nasa 8 (June), 97. https://landsat.usgs.gov/documents/Landsat8DataUsersHandbook.pdf.

Van De Griend, A.A., Owe, M., 1993. On the relationship between thermal emissivity and the normalized difference vegetation index for natural surfaces. Int. J. Rem. Sens. 14 (6), 1119–1131. https://doi.org/10.1080/01431169308904400.

Voogt, J.A., 2000. Image representations of complete urban surface temperatures. Geocarto Int. 15 (3), 21–32. https://doi.org/10.1080/10106040008542160.

Wang, L., Li, C.C., Ying, Q., Cheng, X., Wang, X.Y., Li, X.Y., Hu, L.Y., Liang, L., Yu, L., Huang, H.B., Gong, P., 2012. China's urban expansion from 1990 to 2010 determined with satellite remote sensing. Chin. Sci. Bull. 57 (22), 2802–2812. https://doi.org/10.1007/s11434-012-5235-7.

Waqar, M.M., Mirza, J.F., Mumtaz, R., Hussain, E., 2012. Development of new indices for extraction of built-up area & bare soil. Open Access Sci. Rep. 1 (1), 1–4. https://doi.org/10.4172/scientificreports.13.

Weng, Q., Liu, H., Lu, D., 2007. Assessing the effects of land use and land cover patterns on thermal conditions using landscape metrics in city of Indianapolis, United States. Urban Ecosyst. 10 (2), 203–219. https://doi.org/10.1007/s11252-007-0020-0.

Weng, Q., Lu, D., Schubring, J., 2004. Estimation of land surface temperature-vegetation abundance relationship for urban heat island studies. Remote Sens. Environ. 89 (4), 467–483. https://doi.org/10.1016/j.rse.2003.11.005.

Weng, Q., Yang, S., 2004. Managing the adverse thermal effects of urban development in a densely populated Chinese city. J. Environ. Manag. 70 (2), 145–156. https://doi.org/10.1016/j.jenvman.2003.11.006.

Wilson, J.S., Clay, M., Martin, E., Stuckey, D., Vedder-Risch, K., 2003. Evaluating environmental influences of zoning in urban ecosystems with remote sensing. Remote Sens. Environ. 86 (3), 303–321. https://doi.org/10.1016/S0034-4257(03)00084-1.

Wu, H., Ye, L.P., Shi, W.Z., Clarke, K.C., 2014. Assessing the effects of land use spatial structure on urban heatislands using HJ-1B remote sensing imagery in Wuhan, China. Int. J. Appl. Earth Obs. Geoinf. 32 (1), 67–78. https://doi.org/10.1016/j.jag.2014.03.019.

Xiao, R. bo, Ouyang, Z. yun, Zheng, H., Li, W. feng, Schienke, E.W., Wang, X. ke, 2007. Spatial pattern of impervious surfaces and their impacts on land surface temperature in Beijing, China. J. Environ. Sci. 19 (2), 250–256. https://doi.org/10.1016/S1001-0742(07)60041-2.

Xu, L.Y., Xie, X.D., Li, S., 2013. Correlation analysis of the urban heat island effect and the spatial and temporal distribution of atmospheric particulates using TM images in Beijing. Environ. Pollut. 178, 102–114. https://doi.org/10.1016/j.envpol.2013.03.006.

Xu, Q., Zhang, Y., Li, B., 2014. Recent advances in pansharpening and key problems in applications. Int. J. Image Data Fusion 5 (3), 175–195. https://doi.org/10.1080/19479832.2014.889227.

Xu, R., Zhang, H., Wang, T., Lin, H., 2017. Using pansharpenpansharpened high resolution satellite data to improve impervious surfaces estimation. Int. J. Appl. Earth Obs. Geoinf. 57, 177–189. https://doi.org/10.1016/j.jag.2016.12.020.

Yuan, F., Bauer, M.E., 2007. Comparison of impervious surface area and normalized difference vegetation index as indicators of surface urban heat island effects in Landsat imagery. Remote Sens. Environ. 106 (3), 375–386. https://doi.org/10.1016/j.rse.2006.09.003.

Yuan, F., Sawaya, K.E., Loeffelholz, B.C., Bauer, M.E., 2005. Land cover classification and change analysis of the Twin Cities (Minnesota) metropolitan area by multitemporal Landsat remote sensing. Remote Sens. Environ. 98 (2–3), 317–328. https://doi.org/10.1016/j.rse.2005.08.006.

Zhang, J., Wang, Y., Li, Y., 2006. A C++ program for retrieving land surface temperature from the data of Landsat TM/ETM+ band6. Comput. Geosci. 32 (10), 1796–1805.

Zhang, X., Zhong, T., Feng, X., Wang, K., 2009. Estimation of the relationship between vegetation patches and urban land surface temperature with remote sensing. Int. J. Rem. Sens. 30 (8), 2105–2118. https://doi.org/10.1080/01431160802549252.

Zhang, Y., Mishra, R.K., 2014. From UNB PanSharp to Fuze Go - the success behind the pansharpening algorithm. Int. J. Image Data Fusion 5 (1), 39–53. https://doi.org/10.1080/19479832.2013.848475.

Zhou, W., Huang, G., Cadenasso, M.L., 2011. Does spatial configuration matter? Understanding the effects of land cover pattern on land surface temperature in urban landscapes. Landsc. Urban Plann. 102 (1), 54–63. https://doi.org/10.1016/j.landurbplan.2011.03.009.